THE JOURNAL OF PHYSICAL CHEMISTRY LETTERS
A JOURNAL OF THE AMERICAN CHEMICAL SOCIETY

pubs.acs.org/JPCL

Letter

High-Resolution $^{1}H/^{17}O$ NMR Correlation under Fast Magic-Angle Spinning: Revisiting Cross-Polarization for Quadrupolar Nuclei

Ivan Hung* and Zhehong Gan

Cite This: *J. Phys. Chem. Lett.* 2025, 16, 7036−7041

Read Online

ACCESS | Metrics & More | Article Recommendations

ABSTRACT: An efficient experiment for $^{1}H/^{17}O$ heteronuclear correlation is presented, combining forward-and-back cross-polarization and low-power cosine multiple-quantum magic-angle spinning methods. Double cross-polarization (DCP) is compared with the heteronuclear multiple-quantum correlation (HMQC) method. Both experiments are applicable in instances of enhanced proton polarization such as with dynamic nuclear polarization. Under fast magic-angle spinning, cross-polarization becomes a viable method for polarization transfer and provides an order of magnitude enhancement over HMQC. In particular, it is observed that faster sample spinning opens up regions of *rf* fields optimal for spin-locking and cross-polarization with much less T_2 signal loss. The incorporation of multiple-quantum magic-angle spinning enables high ^{17}O isotropic resolution via proton detection.

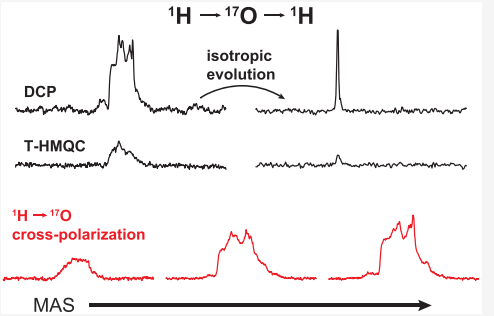

Solid-state nuclear magnetic resonance (NMR) spectroscopy is a powerful technique for the structural characterization of nonliquid compounds. A particular useful feature of solid-state NMR is its ability to identify proximities between nuclei of distinct atomic numbers, i.e., heteronuclear correlation (HETCOR).[1] HETCOR forms an integral component of many NMR methods and is used to great effect in structural biology and chemical applications.[2,3] The most common method for obtaining such correlations is by transfer of polarization between the different species through cross-polarization magic-angle spinning (CPMAS).[4] CPMAS performs impeccably when both nuclear species involved have spin quantum numbers $I = 1/2$. However, when one of the two species is a quadrupolar nucleus (i.e., nuclei with $I > 1/2$), the performance of CP has typically been rather unsatisfactory, largely owing to the inability to efficiently spin-lock quadrupolar nuclei under magic-angle spinning (MAS) because of the large difference in magnitude between the quadrupolar coupling (ν_Q) and the applied *rf* field (ν_1), i.e., $\nu_Q \gg \nu_1$.[5−10] Nevertheless, the ability to characterize quadrupolar nuclei is of great interest because of their ubiquity, making up a large majority of the NMR observable nuclei in the Periodic Table. A particularly interesting target of study in biological systems are the oxygen atoms, which play an integral role in the structure and functions of proteins.[11] Therefore, correlation methods between $I = 1/2$ and quadrupolar nuclei have been developed that, in contrast to CP, apply lengthy pulses *only* to the $I = 1/2$ nuclei, such as dipolar heteronuclear multiple quantum coherence (D-HMQC)[12,13] and dipolar refocused insensitive nuclei enhanced by polarization transfer (D-RINEPT).[14] Aside from the relative difficulty of polarization transfer to and from quadrupolar nuclei, they also display additional anisotropic broadening caused by quadrupole coupling, which is not present for $I = 1/2$ nuclei. It is therefore desirable to develop a HETCOR experiment that can not only provide efficient polarization transfer but also averages out the broadening of the quadrupolar nuclei to achieve isotropic site resolution. To this end, there have been reports of experiments combining HETCOR with multiple-quantum magic-angle spinning (MQMAS) and satellite-transition magic-angle spinning (STMAS), methods that average the quadrupolar broadening.[15−21]

The past couple of decades have seen a significant advance in magic-angle spinning (MAS) technology, allowing experiments to be performed routinely at frequencies at or above 40 kHz, even reaching 200 kHz.[22−25] This progress has led to an outburst of work toward using indirect ^{1}H detection for solid-state NMR spectroscopy in a similar fashion as is commonly employed for NMR of liquids. Faster sample spinning leads to significantly improved line widths and site resolution due to better averaging of homonuclear ^{1}H dipole coupling. And just as for solutions, indirect ^{1}H detection typically provides an enhancement in sensitivity compared to direct detection of the target nuclei.[26,27] Given these advantages, it is of interest to

Received: May 27, 2025
Revised: June 17, 2025
Accepted: June 27, 2025
Published: July 1, 2025

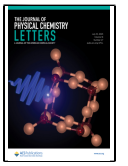

https://doi.org/10.1021/acs.jpclett.5c01621
J. Phys. Chem. Lett. 2025, 16, 7036−7041

develop ^{1}H-detected experiments under fast MAS (≥40 kHz) with indirect *isotropic* observation of quadrupolar nuclei.

It is relevant to note here that the routes of polarization transfer for the aforementioned D-HMQC and D-RINEPT methods differ. The polarization starts from the source nuclei *S*, transit through the recipient nuclei *R*, and return to *S* for D-HMQC (i.e., $S \rightarrow R \rightarrow S$), whereas only a single $S \rightarrow R$ transfer occurs for D-RINEPT just as with conventional one-step CP transfer. Experiments that utilize a single $S \rightarrow R$ transfer for indirect isotropic observation of quadrupolar nuclei developed at slower MAS frequencies[15−17,20,21] have been adapted straightforwardly for fast MAS ^{1}H-detection.[28−30] However, reports of similar experiments using forward-and-back ($S \rightarrow R \rightarrow S$) polarization transfer have been rather scarce, with only a couple of very recent entries that are applicable only to $I = 3/2$ nuclei.[31,32] This work aims to expand the latter type of experiments to half-integer quadrupolar nuclei with $I > 3/2$.

One may be inclined to ask why such an endeavor would be worthwhile. The NMR spectra obtained are essentially the same regardless of which polarization transfer scheme is used, $S \rightarrow R$ or $S \rightarrow R \rightarrow S$. However, the signal-to-noise ratio (s/n) of the spectra achievable per unit of time can be drastically different. The optimal choice between $S \rightarrow R$ and $S \rightarrow R \rightarrow S$ experiments depends strongly on the T_1 relaxation of both nuclei, and the initial polarization of the *S* nuclei. If we take for example the pair of nuclei ^{1}H and ^{17}O, it can often be preferable to perform experiments that begin from ^{17}O polarization (i.e., $^{17}\text{O} \rightarrow {}^{1}\text{H}$) because, although the initial polarization of ^{1}H nuclei is greater than ^{17}O by the ratio of their gyromagnetic ratios (i.e., $\gamma_{^{1}\text{H}}/\gamma_{^{17}\text{O}} \sim 7.4$), ^{17}O T_1 relaxation is often orders of magnitude faster than ^{1}H T_1 due to very efficient ^{17}O quadrupolar relaxation. Thus, a better sensitivity can be obtained as long as $T_1(^{1}\text{H})/T_1(^{17}\text{O}) > (\gamma_{^{1}\text{H}}/\gamma_{^{17}\text{O}})^2 \sim 55$, which is typically a valid assumption in our experience. However, this condition is reversed in cases where (1) the quadrupolar T_1 relaxation is slowed, for example, at low sample temperatures or (2) ^{1}H polarization is enhanced by methods such as dynamic nuclear polarization (DNP).[33,34] Two $S \rightarrow R \rightarrow S$ experiments are examined here for indirectly detected isotropic ^{1}H/^{17}O correlation. In both cases a split-t_1 cos-lpMQMAS[29,35,36] block is used on the ^{17}O channel to achieve isotropic evolution. For the $^{1}\text{H} \rightarrow {}^{17}\text{O} \rightarrow {}^{1}\text{H}$ polarization transfer, the TRAPDOR variant of HMQC (also known as T-HMQC)[37−39] and forward-and-back cross-polarization (also known as double CP, or DCP) are employed. Notably, the D-HMQC method is avoided due to its susceptibility to MAS frequency fluctuations (which causes significant t_1-noise) and the complexities involved in alleviating said t_1-noise.[40,41]

The pulse sequence diagrams and coherence transfer pathways for the two experiments, denoted as ^{iso}T-HMQC and ^{iso}DCP, are shown in Figure 1. One notes that the pulsing scheme for the ^{17}O channel is the same for both experiments: long pulses for $^{1}\text{H} \leftrightarrow {}^{17}\text{O}$ polarization transfer that sandwich a pair of "composite" pulses consisting of a central-transition (CT) selective π-pulse and a satellite-transition (ST) selective "π-pulse" (green cosine pulses). The two composite pulses induce a change in coherence order of $\Delta p = \pm 4$ required for MQMAS of $I = 5/2$ nuclei and are crucial to the efficiency of the experiments.[36] The t_1 evolution is incremented following the split-t_1 method[42] used in MQMAS experiments to average the second-order quadrupolar broadening, i.e., for $I = 5/2$ (a = 19/62, b = 12/62), $I = 7/2$ (a = 101/292, b = 45/292), and $I = 9/2$ (a = 91/254, b = 36/254). The cogwheel phase cycle[43,44] for ^{iso}T-HMQC is $\varphi_1 = \varphi_2 = \varphi_5 = \varphi_6 = 0$, $\varphi_3 = 2n{\cdot}18$, $\varphi_4 = 3n{\cdot}18$, $\varphi_{Rx} = n{\cdot}180$, and for ^{iso}DCP, it is $\varphi_1 = 90$, $\varphi_2 = 180$, $\varphi_3 = 2n{\cdot}18$, $\varphi_4 = 3n{\cdot}18$, $\varphi_5 = \varphi_6 = 0$, $\varphi_{Rx} = n{\cdot}180$, where $n = 0, \ldots, 19$. In both cases, hypercomplex acquisition is performed by decrementing φ_5 and φ_6 simultaneously by 30°.

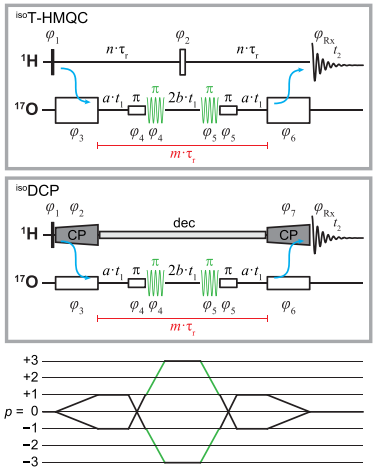

Figure 1. Pulse sequence schematics for the (top) ^{iso}T-HMQC and (bottom) ^{iso}DCP experiments along with a diagram of the coherence transfer pathways selected for the ^{17}O nuclei. Split-t_1 evolution is used to obtain isotropic ^{17}O evolution with the following spin quantum number dependent parameters: $I = 5/2$ (a = 19/62, b = 12/62), $I = 7/2$ (a = 101/292, b = 45/292), and $I = 9/2$ (a = 91/254, b = 36/254). The cogwheel phase cycle[43,44] for ^{iso}T-HMQC is $\varphi_1 = \varphi_2 = \varphi_5 = \varphi_6 = 0$, $\varphi_3 = 2n{\cdot}18$, $\varphi_4 = 3n{\cdot}18$, $\varphi_{Rx} = n{\cdot}180$, and for ^{iso}DCP, it is $\varphi_1 = 90$, $\varphi_2 = 180$, $\varphi_3 = 2n{\cdot}18$, $\varphi_4 = 3n{\cdot}18$, $\varphi_5 = \varphi_6 = 0$, $\varphi_{Rx} = n{\cdot}180$, where $n = 0, \ldots, 19$. In both cases, hypercomplex acquisition is performed by decrementing φ_5 and φ_6 simultaneously by 30°.

All experiments were performed on a sample of 99% ^{13}C and ∼40−45% ^{17}O-enriched calcium oxalate monohydrate (COM) prepared as previously reported,[45] at a magnetic field of 14.1 T using a Bruker Avance NEO spectrometer and a Bruker 1.3 mm HXY MAS probe. A 50 kHz sample spinning frequency (ν_r) was used throughout except where noted in Figure 3. Each T-HMQC TRAPDOR pulse was applied to ^{17}O for 500 μs at an offset of −200 kHz and *rf* field amplitude of $\nu_1 \sim 190$ kHz to achieve $^{1}\text{H}-{}^{17}\text{O}$ dipolar recoupling. While each $^{1}\text{H} \leftrightarrow {}^{17}\text{O}$ CP step used a contact time of 6 ms, and ^{1}H and ^{17}O ν_1 of $0.25\nu_r$ and $0.75\nu_r/3$, respectively, noting that the nutation frequency ν_{nut} for the CT of $I = 5/2$ nuclei such as ^{17}O is related to ν_1 by $\nu_{nut} = (I + 1/2)\nu_1 = 3\nu_1$.[46] Both the CT- and ST-selective ^{17}O π-pulses had durations equal to one rotor period to maintain rotor synchronization of the total t_1 evolution; this is particularly important for the T-HMQC experiment, where otherwise a number of spinning sidebands are observed in the indirect dimension. The CT-selective π-pulses were applied on-resonance with $\nu_1 \sim 8.3$ kHz. The cosine pulses that aim to serve as double-frequency ^{17}O ST-selective "π-pulses" were applied with $\nu_1 \sim 40$ kHz and amplitude-modulation equivalent to frequency offsets of ±550 kHz. It should be noted that the efficiency of the desired $|\pm 1/2\rangle \leftrightarrow |\pm 3/2\rangle$ ST inversion under the experimentally optimized

https://doi.org/10.1021/acs.jpclett.5c01621
J. Phys. Chem. Lett. 2025, 16, 7036−7041

rf field and offset is likely far from that of an ideal ST π-pulse due to the presence of the two sets of satellite-transitions (i.e., $|\pm1/2\rangle \leftrightarrow |\pm3/2\rangle$ and $|\pm3/2\rangle \leftrightarrow |\pm5/2\rangle$) in $I = 5/2$ ^{17}O nuclei and their large frequency distribution.

The efficiency of the ^{iso}T-HMQC and ^{iso}DCP experiments is assessed by acquiring one-dimensional (1D) spectra with $t_1 = 0$. Such ^{1}H-detected spectra are shown in Figure 2a for a sample of COM in comparison to reference spectra and a conventional ^{1}H spin−echo. The reference spectra are acquired by only using the ^{1}H portion of the pulse sequences while keeping all delays, pulse lengths and amplitudes the same as those used for the ^{iso}T-HMQC and ^{iso}DCP spectra. For completeness, spectra acquired *without* isotropic ^{17}O evolution are also shown and denoted as ^{CT}T-HMQC and DCP in Figure 2a. The reference spectra reveal that the T-HMQC experiment (9.6) starts with ∼30% of the signal compared to DCP (29.8) purely because ^{1}H T_2 relaxation is typically much shorter than $T_{1\rho}$ for solid samples. Naturally, this disadvantage propagates to the ^{CT}T-HMQC and DCP spectra after ^{1}H → ^{17}O → ^{1}H forward-and-back transfer, which has an efficiency of slightly more than 3% for both T-HMQC (0.3/9.6 = 3.1%) and DCP (1.0/29.8 = 3.4%). And lastly, the pair of composite pulses used for ^{17}O isotropic evolution have an efficiency of 0.007/0.3 ∼ 2% and 0.08/1.0 ∼ 8% for ^{iso}T-HMQC and ^{iso}DCP, respectively. The lower efficiency observed for ^{iso}T-HMQC is likely due to destructive interference between the ST-selective π-pulses and the anisotropic phase generated by the TRAPDOR pulses; this is a subject of ongoing investigation. It should be noted that the efficiency of all the T-HMQC and DCP experiments is directly affected by the ^{17}O enrichment level, ∼40% in this case; thus, the values quoted above should be increased by a factor of 2.5 to obtain a proper assessment of their performance. On the whole, it is observed in this instance that the ^{iso}DCP experiment performs an order of magnitude better than ^{iso}T-HMQC. ^{iso}DCP is expected to outperform ^{iso}T-HMQC in sensitivity under most circumstances, partly because $T_{1\rho}$ is typically much longer than T_2 in solids. And also because, for T-HMQC, the polarization of the source nuclei is distributed to all possible coherences of the quadrupolar nuclei instead of only the single-quantum CT coherence,[39] which leads to a sizable loss of sensitivity that increases with the spin quantum number. A potential drawback of DCP may be its offset dependence due to the use of relatively low *rf* amplitudes, in contrast to T-HMQC, which instead employs very high *rf* fields. In our experience, the bandwidth of DCP is approximately equal to the nutation frequency applied to the quadrupolar nuclei; $\nu_{nut}(^{17}O) \sim 38$ kHz in the current example, which translates to ∼460 ppm at 14.1 T, or ∼350 ppm at 18.8 T, and should be sufficient to cover the chemical shift range of ^{17}O sites under most circumstances. Unsurprisingly, the sensitivity advantage of DCP over T-HMQC observed in the 1D spectra carries over directly to the 2D spectra (Figure 2b). Notably, the reduced signal observed for the 1D ^{iso}DCP spectrum compared to the DCP spectrum is compensated by the concentration of intensity into sharp isotropic peaks in the 2D ^{iso}DCP spectrum (1.09), which results in a similar s/n compared to the 2D DCP spectrum (1.00). This is in agreement with what has previously been observed in a model dipeptide sample.[29] Aside from a sensitivity advantage, DCP is also superior to T-HMQC for multidimensional experiments because the indirect dimensions are not influenced by ^{1}H T_2 relaxation, and also heteronuclear ^{1}H decoupling can be applied in a straightforward fashion when necessary, resulting in a general resolution advantage for DCP.

Having obtained positive results for ^{1}H/^{17}O correlation using cross-polarization both here and in previous reports,[29,30] it is of interest to examine/document further the performance of ^{1}H ↔ ^{17}O CP and the reason why it is often dismissed as a viable method for polarization transfer. To this end, the performance of 1 ms on-resonance spin-locking after excitation by a $\pi/2$-pulse for the ^{1}H and ^{17}O nuclei was measured as a function of ν_{nut} at three MAS frequencies of ν_r = 12.5, 25, and 50 kHz (Figure 3). For clarity, the reader is reminded that $\nu_{nut} = (I + 1/2)\nu_1$. The rotary resonance recoupling (R^3) conditions ($\nu_{nut} = n\nu_r$, n = 1/2, 1, 2),[47−51] where dipolar coupling and chemical shift anisotropy averaged by MAS are reintroduced, give rise to valleys of ^{1}H signal loss, most clearly observed at 50 kHz MAS (Figure 3a, green vertical lines). Minor dips are also observed due to high-order recoupling

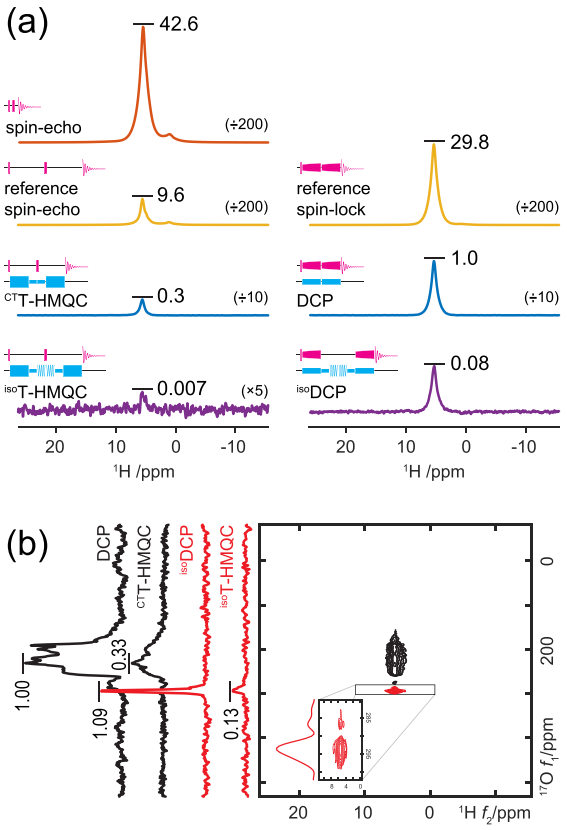

Figure 2. (a) Comparison of ^{1}H-detected 1D NMR spectra of ∼40% ^{17}O-enriched calcium oxalate monohydrate (COM). The maximum signal intensity normalized to the DCP spectrum is shown for each spectrum. The spin−echo spectrum was acquired with a one rotor-period interpulse delay, while other spectra were acquired with the same parameters optimized for the ^{iso}T-HMQC and ^{iso}DCP spectra. All spectra were acquired by averaging the same number of transients. (b) Comparison of isotropic (red) and anisotropic (black) ^{17}O-evolved 2D ^{1}H/^{17}O T-HMQC and DCP NMR spectra of COM. Projections of the indirect ^{17}O dimension are shown to the left along with the normalized s/n of the spectra. Each 2D spectrum was acquired with a 1 s recycle delay, 256 complex t_1 points, and 20 averaged transients, resulting in experimental times of ∼2.8 h. The inset shows an expansion of the isotropic peaks in the 2D ^{iso}DCP spectrum.

https://doi.org/10.1021/acs.jpclett.5c01621
J. Phys. Chem. Lett. 2025, 16, 7036−7041

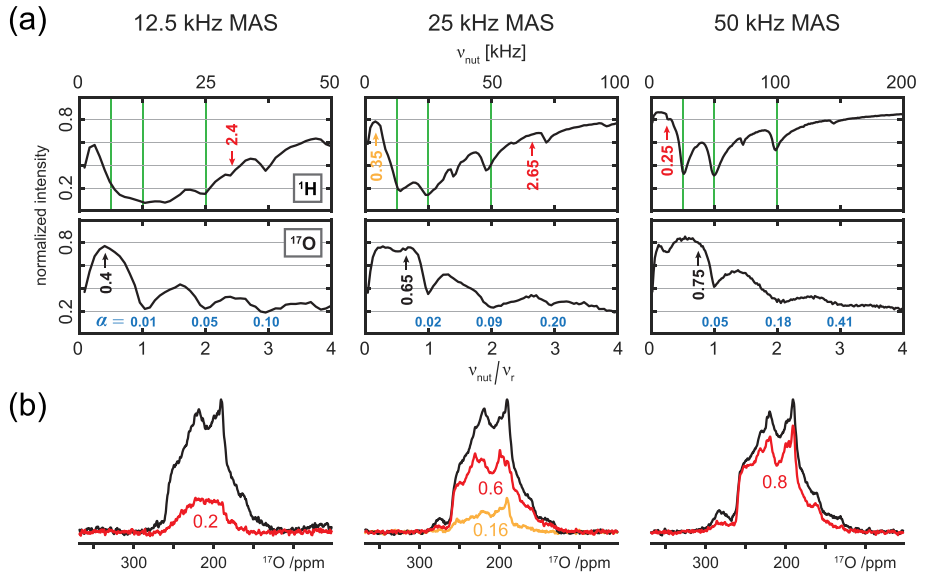

Figure 3. (a) Spin-lock intensity of COM as a function of *rf* nutation frequency ν_{nut} at three different MAS frequencies: 12.5 (left column), 25 (middle column), and 50 kHz (right column). The intensities are shown normalized to the intensity of a direct excitation spectrum, while the ν_{nut} values are normalized to the applied MAS frequency ν_r. Green vertical lines denote the positions of the R^3 conditions. For reference, the value of the adiabaticity parameter α is shown in blue for the ^{17}O curves. (b) $^1H \rightarrow {}^{17}O$ CPMAS NMR spectra (red and yellow traces) of COM acquired using the ν_{nut} values shown in (a), as compared to the direct-excitation ^{17}O spectra (black traces), acquired at the same MAS frequency and with the same number of averaged transients. For reference, the ^{17}O sites in the COM sample have an average C_Q of ∼7.3 MHz.[45]

conditions,[52,53] which are not addressed further here. At slower spinning frequencies the R^3 valleys broaden so much that they merge together, leading to significant signal loss over most ν_{nut} values, with only ∼60% of the signal remaining at 12.5 kHz MAS. Whereas for ^1H the spin-lock efficiency is typically best at higher *rf* field amplitudes, the situation is reversed for ^{17}O nuclei, which shows a maximum at $\nu_{nut} < \nu_r$ followed by progressively worse signal loss as ν_{nut} increases. Notably, the ^{17}O spin-lock efficiency curves display a very similar pattern at the three different MAS frequencies and do not conform appreciably to description by the adiabaticity parameter introduced by Vega;[5,6] $\alpha = \nu_{nut}^2/(\nu_r \cdot \nu_Q)$, where $\nu_Q = 3C_Q/[2I(2I-1)]$ and C_Q is the quadrupolar coupling constant. But instead, they appear to depend solely on the ratio between ν_{nut} and ν_r. The loss of spin lock with increased ν_{nut} is caused by crossings of the *rf* and ST frequencies brought about by MAS. During these crossings, on-resonance *rf* for both the CT and STs induces coherence transfer between the two transitions and causes loss of CT polarization. The rate of polarization leakage is proportional to the square of the *rf* field; therefore efficient spin-lock can be maintained only at lower *rf* fields.

The matching conditions for effective CP under MAS (i.e., $\nu_{nut}(^1H) \pm \nu_{nut}(^{17}O) = |n\nu_r|$ with $n = 1, 2$)[4,54−56] restrict the difference between $\nu_{nut}(^1H)$ and $\nu_{nut}(^{17}O)$ to be no more than $2\nu_r$. Since ^{17}O spin-locking is only effective below ν_r, it is only possible to perform $^1H \leftrightarrow {}^{17}O$ CP efficiently using ^1H ν_{nut} values less than $3\nu_r$. A survey of the plots in Figure 3a allows selection of ν_{nut} values for $^1H \leftrightarrow {}^{17}O$ CP that provide the most effective spin-locking for both nuclei and avoid R^3 signal loss conditions. $^1H \rightarrow {}^{17}O$ CPMAS NMR spectra of COM using the optimal ν_{nut} values found are shown in Figure 3b in comparison to directly excited ^{17}O spectra. A few salient features of note: at 12.5 kHz MAS, spin-locking is rather inefficient for both nuclei, particularly for ^1H nuclei, largely due to the low *rf* field amplitudes available for CP at this MAS frequency. A compromise must be made between better spin-locking for the ^1H or ^{17}O nuclei, both of which result in poor CP. At 25 kHz MAS, improved averaging of $^1H-{}^1H$ dipolar coupling narrows the R^3 conditions and increases the ^1H spin-lock efficiency throughout the $\nu_{nut}(^1H)$ range. Additionally, the range of viable $\nu_{nut}(^{17}O)$ broadens, allowing the *rf* fields for both nuclei to be increased slightly, which yields a much improved $^1H \rightarrow {}^{17}O$ CP spectrum (red trace) using a similar zero-quantum (ZQ) condition of $\nu_{nut}(^1H) - \nu_{nut}(^{17}O) = 2\nu_r$, as for the lower MAS frequency. A low *rf* ^1H spin-lock condition also emerges at $\nu_{nut}(^1H) \sim 0.35\nu_r$, which appears to be more effective than at higher *rf* fields. However, use of this value to fulfill the double-quantum (DQ) CP condition $\nu_{nut}(^1H) + \nu_{nut}(^{17}O) = \nu_r$ does not yield the CP spectrum (yellow trace) expected from the spin-lock efficiencies. The lower signal from using DQ-CP may be due to a greater decay in ^1H spin-lock efficiency at low versus high *rf* fields when using long contact times, as only a $\nu_{nut}(^1H)$ of ∼8 kHz is applied in that case. Upon further increase of the MAS frequency to 50 kHz, the use of low *rf* conditions becomes fully realized, as has already been reported in the literature for CP, decoupling, and recoupling.[57−59] The $^1H \rightarrow {}^{17}O$ CP spectrum approaches the intensity of the direct ^{17}O excitation spectrum. Thus, in all, the increase in MAS from 12.5 to 50 kHz results in a 4-fold increase in CP efficiency, and reinforces why the majority of NMR studies of quadrupolar nuclei, which are typically performed at slower MAS frequencies, tend to avoid application of CP for signal enhancement or polarization transfer.

AUTHOR INFORMATION

Corresponding Author

Ivan Hung − *National High Magnetic Field Laboratory, Tallahassee, Florida 32310, United States;* orcid.org/0000-0001-8916-739X; Email: hung@magnet.fsu.edu

https://doi.org/10.1021/acs.jpclett.5c01621
J. Phys. Chem. Lett. 2025, 16, 7036−7041

Author

Zhehong Gan − *National High Magnetic Field Laboratory, Tallahassee, Florida 32310, United States;* orcid.org/0000-0002-9855-5113

Complete contact information is available at: https://pubs.acs.org/10.1021/acs.jpclett.5c01621

Notes

The authors declare no competing financial interest.

■ ACKNOWLEDGMENTS

Drs. Ieva Goldberga and Danielle Laurencin (ICGM, France) are acknowledged for generously providing the sample of ^{17}O-enriched calcium oxalate monohydrate. This work was supported by the National High Magnetic Field Laboratory (NHMFL, USA) through NSF DMR-2128556 and the State of Florida. Use of the NHMFL NMR facility is available free of charge; for more information please visit https://nationalmaglab.org/user-facilities/nmr-mri.

■ REFERENCES

(1) Maudsley, A. A.; Ernst, R. R. Indirect Detection of Magnetic Resonance by Heteronuclear Two-Dimensional Spectroscopy. *Chem. Phys. Lett.* **1977**, *50* (3), 368−372.

(2) Baldus, M. ICMRBS Founder's Medal 2006: Biological Solid-State NMR. *Methods and Applications. J. Biomol. NMR* **2007**, *39* (1), 73−86.

(3) Comellas, G.; Rienstra, C. M. Protein Structure Determination by Magic-Angle Spinning Solid-State NMR, and Insights into the Formation, Structure, and Stability of Amyloid Fibrils. *Annu. Rev. Biophys.* **2013**, *42* (1), 515−536.

(4) Stejskal, E. O.; Schaefer, J.; Waugh, J. S. Magic-Angle Spinning and Polarization Transfer in Proton-Enhanced NMR. *J. Magn. Reson.* **1977**, *28* (1), 105−112.

(5) Vega, A. J. MAS NMR Spin Locking of Half-Integer Quadrupolar Nuclei. *J. Magn. Reson.* **1992**, *96* (1), 50−68.

(6) Vega, A. J. CP/MAS of Quadrupolar S = 3/2 Nuclei. *Solid State Nucl. Magn. Reson.* **1992**, *1* (1), 17−32.

(7) Zhang, Y.; Deng, F.; Qiu, J.; Ye, C. Spin-Locking Mechanism of Spin I = 3/2 Quadrupolar Nuclei Undergo Magic Angle Spinning. *Solid State Nucl. Magn. Reson.* **2000**, *15*, 209−216.

(8) Baldus, M.; Rovnyak, D.; Griffin, R. G. Radio-Frequency-Mediated Dipolar Recoupling among Half-Integer Quadrupolar Spins. *J. Chem. Phys.* **2000**, *112* (13), 5902−5909.

(9) Amoureux, J.-P.; Pruski, M. Theoretical and Experimental Assessment of Single- and Multiple-Quantum Cross-Polarization in Solid State NMR. *Mol. Phys.* **2002**, *100* (10), 1595−1613.

(10) Ashbrook, S. E.; Wimperis, S. Spin-Locking of Half-Integer Quadrupolar Nuclei in Nuclear Magnetic Resonance of Solids: Second-Order Quadrupolar and Resonance Offset Effects. *J. Chem. Phys.* **2009**, *131* (19), No. 194509.

(11) Wu, G. ^{17}O NMR Studies of Organic and Biological Molecules in Aqueous Solution and in the Solid State. *Prog. Nucl. Magn. Reson. Spectrosc.* **2019**, *114*−*115*, 135−191.

(12) Gan, Z. H.; Amoureux, J. P.; Trebosc, J. Proton-Detected N-14 MAS NMR Using Homonuclear Decoupled Rotary Resonance. *Chem. Phys. Lett.* **2007**, *435* (1−3), 163−169.

(13) Cavadini, S.; Abraham, A.; Bodenhausen, G. Proton-Detected Nitrogen-14 NMR by Recoupling of Heteronuclear Dipolar Interactions Using Symmetry-Based Sequences. *Chem. Phys. Lett.* **2007**, *445* (1−3), 1−5.

(14) Trebosc, J.; Hu, B.; Amoureux, J. P.; Gan, Z. Through-Space R^3-HETCOR Experiments between Spin-1/2 and Half-Integer Quadrupolar Nuclei in Solid-State NMR. *J. Magn. Reson.* **2007**, *186* (2), 220−227.

(15) Wang, S. H.; De Paul, S. M.; Bull, L. M. High-Resolution Heteronuclear Correlation between Quadrupolar and Spin-1/2 Nuclei Using Multiple-Quantum Magic-Angle Spinning. *J. Magn. Reson.* **1997**, *125* (2), 364−368.

(16) Chan, J. C. C. High-Resolution Heteronuclear Correlation between Quadrupolar Nuclei. *J. Magn. Reson.* **1999**, *140* (2), 487−490.

(17) Mali, G.; Amoureux, J.-P.; Kaučič, V. ^{27}Al→^{31}P 3QMAS/HETCOR Experiment in Aluminophosphate Molecular Sieves. *Phys. Chem. Chem. Phys.* **2000**, *2* (24), 5737−5742.

(18) Siegel, R.; Rocha, J.; Mafra, L. Combining STMAS and CRAMPS NMR Spectroscopy: High-Resolution HETCOR NMR Spectra of Quadrupolar and ^{1}H Nuclei in Solids. *Chem. Phys. Lett.* **2009**, *470* (4−6), 337−341.

(19) Trébosc, J.; Lafon, O.; Hu, B.; Amoureux, J.-P. Indirect High-Resolution Detection for Quadrupolar Spin-3/2 Nuclei in Dipolar HMQC Solid-State NMR Experiments. *Chem. Phys. Lett.* **2010**, *496* (1−3), 201−207.

(20) Martineau, C.; Bouchevreau, B.; Taulelle, F.; Trébosc, J.; Lafon, O.; Amoureux, J.-P. High-Resolution through-Space Correlations between Spin-1/2 and Half-Integer Quadrupolar Nuclei Using the MQ-D-R-INEPT NMR Experiment. *Phys. Chem. Chem. Phys.* **2012**, *14* (19), 7112.

(21) Hung, I.; Gan, Z.; Wu, G. Two- and Three-Dimensional ^{13}C−^{17}O Heteronuclear Correlation NMR Spectroscopy for Studying Organic and Biological Solids. *J. Phys. Chem. Lett.* **2021**, *12* (36), 8897−8902.

(22) Paulson, E. K.; Morcombe, C. R.; Gaponenko, V.; Dancheck, B.; Byrd, R. A.; Zilm, K. W. Sensitive High Resolution Inverse Detection NMR Spectroscopy of Proteins in the Solid State. *J. Am. Chem. Soc.* **2003**, *125* (51), 15831−15836.

(23) Demers, J.-P.; Chevelkov, V.; Lange, A. Progress in Correlation Spectroscopy at Ultra-Fast Magic-Angle Spinning: Basic Building Blocks and Complex Experiments for the Study of Protein Structure and Dynamics. *Solid State Nucl. Magn. Reson.* **2011**, *40* (3), 101−113.

(24) Le Marchand, T.; Schubeis, T.; Bonaccorsi, M.; Paluch, P.; Lalli, D.; Pell, A. J.; Andreas, L. B.; Jaudzems, K.; Stanek, J.; Pintacuda, G. ^{1}H-Detected Biomolecular NMR under Fast Magic-Angle Spinning. *Chem. Rev.* **2022**, *122* (10), 9943−10018.

(25) Nishiyama, Y.; Hou, G.; Agarwal, V.; Su, Y.; Ramamoorthy, A. Ultrafast Magic Angle Spinning Solid-State NMR Spectroscopy: Advances in Methodology and Applications. *Chem. Rev.* **2023**, *123* (3), 918−988.

(26) Ishii, Y.; Tycko, R. Sensitivity Enhancement in Solid State ^{15}N NMR by Indirect Detection with High-Speed Magic Angle Spinning. *J. Magn. Reson.* **2000**, *142* (1), 199−204.

(27) Venkatesh, A.; Ryan, M. J.; Biswas, A.; Boteju, K. C.; Sadow, A. D.; Rossini, A. J. Enhancing the Sensitivity of Solid-State NMR Experiments with Very Low Gyromagnetic Ratio Nuclei with Fast Magic Angle Spinning and Proton Detection. *J. Phys. Chem. A* **2018**, *122* (25), 5635−5643.

(28) Sasaki, A.; Trébosc, J.; Amoureux, J.-P. A Comparison of Through-Space Population Transfers from Half-Integer Spin Quadrupolar Nuclei to ^{1}H Using MQ-HETCOR and MQ-SPAM-HETCOR under Fast MAS. *J. Magn. Reson.* **2021**, *329*, No. 107028.

(29) Hung, I.; Keeler, E. G.; Mao, W.; Gor'kov, P. L.; Griffin, R. G.; Gan, Z. Residue-Specific High-Resolution ^{17}O Solid-State Nuclear Magnetic Resonance of Peptides: Multidimensional Indirect 1H Detection and Magic-Angle Spinning. *J. Phys. Chem. Lett.* **2022**, *13* (28), 6549−6558.

(30) Hung, I.; Mao, W.; Keeler, E. G.; Griffin, R. G.; Gor'kov, P. L.; Gan, Z. Characterization of Peptide O···HN Hydrogen Bonds via ^{1}H-Detected ^{15}N/^{17}O Solid-State NMR Spectroscopy. *Chem. Commun.* **2023**, *59* (21), 3111−3113.

(31) Pandey, M. K.; Nishiyama, Y. High-Resolution Heteronuclear Correlations between Spin-1/2 and Half-Integer Quadrupolar Nuclei under Fast MAS Solid-State NMR. *Biophys. Chem.* **2024**, *310*, No. 107254.

(32) Trébosc, J.; Lafon, O.; Amoureux, J.-P. High-Resolution Indirect Detection of Spin-3/2 Quadrupolar Nuclei in Solids Using Multiple-Quantum-Filtered through-Space D-HMQC Experiments. *Solid State Nucl. Magn. Reson.* **2024**, *134*, No. 101971.
(33) Becerra, L. R.; Gerfen, G. J.; Temkin, R. J.; Singel, D. J.; Griffin, R. G. Dynamic Nuclear Polarization with a Cyclotron Resonance Maser at 5 T. *Phys. Rev. Lett.* **1993**, *71* (21), 3561−3564.
(34) Maly, T.; Debelouchina, G. T.; Bajaj, V. S.; Hu, K.-N.; Joo, C.-G.; Mak-Jurkauskas, M. L.; Sirigiri, J. R.; van der Wel, P. C. A.; Herzfeld, J.; Temkin, R. J.; Griffin, R. G. Dynamic Nuclear Polarization at High Magnetic Fields. *J. Chem. Phys.* **2008**, *128* (5), No. 052211.
(35) Hung, I.; Gan, Z. Isotropic Solid-State MQMAS NMR Spectra for Large Quadrupolar Interactions Using Satellite-Transition Selective Inversion Pulses and Low Rf Fields. *J. Magn. Reson.* **2021**, *324*, No. 106913.
(36) Hung, I.; Gan, Z. On the Use of Single-Frequency versus Double-Frequency Satellite-Transition Pulses for MQMAS. *J. Magn. Reson.* **2021**, *328*, No. 106994.
(37) Jarvis, J. A.; Haies, I. M.; Williamson, P. T. F.; Carravetta, M. An Efficient NMR Method for the Characterisation of ^{14}N Sites through Indirect ^{13}C Detection. *Phys. Chem. Chem. Phys.* **2013**, *15* (20), 7613.
(38) Hung, I.; Gor'kov, P.; Gan, Z. Efficient and Sideband-Free ^{1}H-Detected ^{14}N Magic-Angle Spinning NMR. *J. Chem. Phys.* **2019**, *151* (15), No. 154202.
(39) Hung, I.; Gan, Z. High Resolution NMR of S = 3/2 Quadrupole Nuclei by Detection of Double-Quantum Satellite-Transitions via Protons. *J. Phys. Chem. Lett.* **2020**, *11* (12), 4734−4740.
(40) Venkatesh, A.; Luan, X.; Perras, F. A.; Hung, I.; Huang, W.; Rossini, A. J. t_1-Noise Eliminated Dipolar Heteronuclear Multiple-Quantum Coherence Solid-State NMR Spectroscopy. *Phys. Chem. Chem. Phys.* **2020**, *22* (36), 20815−20828.
(41) Perras, F. A.; Goh, T. W.; Huang, W. t_1-Noise Elimination by Continuous Chemical Shift Anisotropy Refocusing. *Solid State Nucl. Magn. Reson.* **2022**, *120*, No. 101807.
(42) Brown, S. P.; Wimperis, S. Two-Dimensional Multiple-Quantum MAS NMR of Quadrupolar Nuclei: A Comparison of Methods. *J. Magn. Reson.* **1997**, *128* (1), 42−61.
(43) Levitt, M. H.; Madhu, P. K.; Hughes, C. E. Cogwheel Phase Cycling. *J. Magn. Reson.* **2002**, *155* (2), 300−306.
(44) Jerschow, A.; Kumar, R. Calculation of Coherence Pathway Selection and Cogwheel Cycles. *J. Magn. Reson.* **2003**, *160* (1), 59−64.
(45) Goldberga, I.; Hung, I.; Sarou-Kanian, V.; Gervais, C.; Gan, Z.; Novák-Špačková, J.; Métro, T.-X.; Leroy, C.; Berthomieu, D.; Van Der Lee, A.; Bonhomme, C.; Laurencin, D. High-Resolution ^{17}O Solid-State NMR as a Unique Probe for Investigating Oxalate Binding Modes in Materials: The Case Study of Calcium Oxalate Biominerals. *Inorg. Chem.* **2024**, *63* (22), 10179−10193.
(46) Wu, D. H.; Sanctuary, B. C. Reduction and Suppression of the Nuclear Quadrupole Interaction in Solids by NMR Strong Nutation Spectroscopy. *J. Magn. Reson. A* **1993**, *103* (2), 171−174.
(47) Raleigh, D. P.; Levitt, M. H.; Griffin, R. G. Rotational Resonance in Solid-State NMR. *Chem. Phys. Lett.* **1988**, *146* (1−2), 71−76.
(48) Oas, T. G.; Griffin, R. G.; Levitt, M. H. Rotary Resonance Recoupling of Dipolar Interactions in Solid-State Nuclear Magnetic-Resonance Spectroscopy. *J. Chem. Phys.* **1988**, *89* (2), 692−695.
(49) Gan, Z. H.; Grant, D. M. Rotational Resonance in a Spin-Lock Field for Solid-State NMR. *Chem. Phys. Lett.* **1990**, *168* (3−4), 304−308.
(50) Nielsen, N. C.; Bildsoe, H.; Jakobsen, H. J.; Levitt, M. H. Double-Quantum Homonuclear Rotary Resonance - Efficient Dipolar Recovery in Magic-Angle-Spinning Nuclear-Magnetic-Resonance. *J. Chem. Phys.* **1994**, *101* (3), 1805−1812.
(51) Verel, R.; Baldus, M.; Ernst, M.; Meier, B. H. A Homonuclear Spin-Pair Filter for Solid-State NMR Based on Adiabatic-Passage Techniques. *Chem. Phys. Lett.* **1998**, *287* (3−4), 421−428.
(52) Lange, A.; Scholz, I.; Manolikas, T.; Ernst, M.; Meier, B. H. Low-Power Cross Polarization in Fast Magic-Angle Spinning NMR Experiments. *Chem. Phys. Lett.* **2009**, *468* (1−3), 100−105.
(53) Demers, J. P.; Vijayan, V.; Becker, S.; Lange, A. Tailored Low-Power Cross-Polarization under Fast Magic-Angle Spinning. *J. Magn. Reson.* **2010**, *205* (2), 216−223.
(54) Sardashti, M.; Maciel, G. E. Effects of Sample Spinning on Cross Polarization. *J. Magn. Reson.* **1987**, *72* (3), 467−474.
(55) Wind, R. A.; Dec, S. F.; Lock, H.; Maciel, G. E. C-13 CP Mas and High-Speed Magic-Angle Spinning. *J. Magn. Reson.* **1988**, *79* (1), 136−139.
(56) Meier, B. H. Cross Polarization under Fast Magic Angle Spinning - Thermodynamical Considerations. *Chem. Phys. Lett.* **1992**, *188* (3−4), 201−207.
(57) Laage, S.; Marchetti, A.; Sein, J.; Pierattelli, R.; Sass, H. J.; Grzesiek, S.; Lesage, A.; Pintacuda, G.; Emsley, L. Band-Selective H-1-C-13 Cross-Polarization in Fast Magic Angle Spinning Solid-State NMR Spectroscopy. *J. Am. Chem. Soc.* **2008**, *130* (51), 17216−17217.
(58) Kotecha, M.; Wickramasinghe, N. P.; Ishii, Y. Efficient Low-Power Heteronuclear Decoupling in ^{13}C High-Resolution Solid-State NMR under Fast Magic Angle Spinning. *Magn. Reson. Chem.* **2007**, *45* (S1), S221−S230.
(59) Tan, K. O.; Agarwal, V.; Lakomek, N.-A.; Penzel, S.; Meier, B. H.; Ernst, M. Efficient Low-Power TOBSY Sequences for Fast MAS. *Solid State Nucl. Magn. Reson.* **2018**, *89*, 27−34.

https://doi.org/10.1021/acs.jpclett.5c01621
J. Phys. Chem. Lett. 2025, 16, 7036−7041